Efficient coupling of double-metal terahertz quantum cascade lasers to flexible dielectric-lined hollow metallic waveguides

R. Wallis,[1,*] R. Degl'Innocenti,[1] D. S. Jessop,[1] Y. Ren,[1] A. Klimont,[1] Y. D. Shah,[1] O. Mitrofanov,[2] C. M. Bledt,[3] J. E. Melzer,[3] J. A. Harrington,[3] H. E. Beere,[1] and D. A. Ritchie[1]

[1]Cavendish Laboratory, University of Cambridge, J J Thomson Avenue, Cambridge, CB3 0HE, UK
[2]Department of Electronic and Electrical Engineering, University College London, Torrington Place, London, WC1E 7JE, UK
[3]School of Engineering, Rutgers University, 607 Taylor Road, Piscataway, New Jersey 08854, USA
[*]rw497@cam.ac.uk

Abstract: The growth in terahertz frequency applications utilising the quantum cascade laser is hampered by a lack of targeted power delivery solutions over large distances (>100 mm). Here we demonstrate the efficient coupling of double-metal quantum cascade lasers into flexible polystyrene lined hollow metallic waveguides via the use of a hollow copper waveguide integrated into the laser mounting block. Our approach exhibits low divergence, Gaussian-like emission, which is robust to misalignment error, at distances > 550 mm, with a coupling efficiency from the hollow copper waveguide into the flexible waveguide > 90%. We also demonstrate the ability to nitrogen purge the flexible waveguide, increasing the power transmission by up to 20% at 2.85 THz, which paves the way for future fibre based terahertz sensing and spectroscopy applications.

OCIS codes: (140.5965) Semiconductor lasers, quantum cascade; (230.7370) Waveguides; (140.3300) Laser beam shaping.

References and links

1. R. Köhler, A. Tredicucci, F. Beltram, H. E. Beere, E. H. Linfield, A. G. Davies, D. A. Ritchie, R. C. Iotti, and F. Rossi, "Terahertz semiconductor-heterostructure laser," Nature **417**(6885), 156–159 (2002).
2. M. Tonouchi, "Cutting-edge terahertz technology," Nat. Photonics **1**(2), 97–105 (2007).
3. A. Valavanis, J. Zhu, J. Freeman, L. Li, L. Chen, A. G. Davies, E. H. Linfield, and P. Dean, "Terahertz quantum cascade lasers with >1 W output powers," Electron. Lett. **50**(4), 309–311 (2014).
4. M. Rösch, G. Scalari, M. Beck, and J. Faist, "Octave-spanning semiconductor laser," Nat. Photonics **9**(1), 42–47 (2014).
5. O. Mitrofanov, R. James, F. A. Fernandez, T. K. Mavrogordatos, and J. A. Harrington, "Reducing transmission losses in hollow THz waveguides," IEEE Trans. THz Sci. Tech. **1**(1), 124–132 (2011).
6. H. Han, H. Park, M. Cho, and J. Kim, "Terahertz pulse propagation in a plastic photonic crystal fiber," Appl. Phys. Lett. **80**(15), 2634–2636 (2002).
7. A. Hassani, A. Dupuis, and M. Skorobogatiy, "Low loss porous terahertz fibers containing multiple subwavelength holes," Appl. Phys. Lett. **92**(7), 071101 (2008).
8. B. Bowden, J. A. Harrington, and O. Mitrofanov, "Silver/polystyrene-coated hollow glass waveguides for the transmission of terahertz radiation," Opt. Lett. **32**(20), 2945–2947 (2007).
9. M. Navarro-Cía, M. S. Vitiello, C. M. Bledt, J. E. Melzer, J. A. Harrington, and O. Mitrofanov, "Terahertz wave transmission in flexible polystyrene-lined hollow metallic waveguides for the 2.5-5 THz band," Opt. Express **21**(20), 23748–23755 (2013).
10. O. Mitrofanov and J. A. Harrington, "Dielectric-lined cylindrical metallic THz waveguides: mode structure and dispersion," Opt. Express **18**(3), 1898–1903 (2010).
11. B. Bowden, J. A. Harrington, and O. Mitrofanov, "Low-loss modes in hollow metallic terahertz waveguides with dielectric coatings," Appl. Phys. Lett. **93**(18), 181104 (2008).
12. B. S. Williams, S. Kumar, H. Callebaut, Q. Hu, and J. L. Reno, "Terahertz quantum-cascade laser at λ≈100 μm using metal waveguide for mode confinement," Appl. Phys. Lett. **83**(11), 2124 (2003).
13. M. S. Vitiello, J. H. Xu, M. Kumar, F. Beltram, A. Tredicucci, O. Mitrofanov, H. E. Beere, and D. A. Ritchie, "High efficiency coupling of Terahertz micro-ring quantum cascade lasers to the low-loss optical modes of hollow metallic waveguides," Opt. Express **19**(2), 1122–1130 (2011).

#241983 Received 8 Jun 2015; revised 7 Sep 2015; accepted 8 Sep 2015; published 29 Sep 2015

Corrected: 22 October 2015

14. M. S. Vitiello, J. Xu, F. Beltram, A. Tredicucci, O. Mitrofanov, J. A. Harrington, H. E. Beere, and D. A. Ritchie, "Guiding a terahertz quantum cascade laser into a flexible silver-coated waveguide," Appl. Phys. Lett. **110**(6), 063112 (2011).
15. M. I. Amanti, M. Fischer, G. Scalari, M. Beck, and J. Faist, "Low-divergence single-mode terahertz quantum cascade laser," Nat. Photonics **3**(10), 586–590 (2009).
16. A. Wei Min Lee, Q. Qin, S. Kumar, B. S. Williams, Q. Hu, and J. L. Reno, "High-power and high-temperature THz quantum-cascade lasers based on lens-coupled metal-metal waveguides," Opt. Lett. **32**(19), 2840–2842 (2007).
17. M. I. Amanti, M. Fischer, C. Walther, G. Scalari, and J. Faist, "Horn antennas for terahertz quantum cascade lasers," Electron. Lett. **43**(10), 573–574 (2007).
18. A. Brewer, J. R. Freeman, P. Cavalié, J. Maysonnave, J. Tignon, S. S. Dhillon, H. E. Beere, and D. A. Ritchie, "Coherent detection of metal-metal terahertz quantum cascade lasers with improved emission characteristics," Appl. Phys. Lett. **104**(8), 081107 (2014).
19. J. Lloyd-Hughes, G. Scalari, A. van Kolck, M. Fischer, M. Beck, and J. Faist, "Coupling terahertz radiation between sub-wavelength metal-metal waveguides and free space using monolithically integrated horn antennae," Opt. Express **17**(20), 18387–18393 (2009).
20. W. Maineult, P. Gellie, A. Andronico, P. Filloux, G. Leo, C. Sirtori, S. Barbieri, E. Peytavit, T. Akalin, J. Lampin, H. E. Beere, and D. A. Ritchie, "Metal-metal terahertz quantum cascade laser with micro-transverse-electromagnetic-horn antenna," Appl. Phys. Lett. **93**(18), 183508 (2008).
21. R. Degl'Innocenti, Y. D. Shah, D. S. Jessop, Y. Ren, O. Mitrofanov, H. E. Beere, and D. A. Ritchie, "Hollow metallic waveguides integrated with terahertz quantum cascade lasers," Opt. Express **22**(20), 24439–24449 (2014).
22. F. Castellano, L. Li, E. H. Linfield, A. G. Davies, H. E. Beere, D. A. Ritchie, and M. S. Vitiello, "THz waveguide adapters for efficient radiation out-coupling from double metal THz QCLs," Opt. Express **23**(4), 5190–5200 (2015).
23. M. Saito and K. Kikuchi, "Infrared optical fiber sensors," Opt. Rev. **4**(5), 527–538 (1997).
24. S. Barbieri, J. Alton, H. E. Beere, J. Fowler, E. H. Linfield, and D. A. Ritchie, "2.9 THz quantum cascade lasers operating up to 70K in continuous wave," Appl. Phys. Lett. **85**(10), 1674 (2004).
25. M. I. Amanti, G. Scalari, R. Terazzi, M. Fischer, M. Beck, J. Faist, A. Rudra, P. Gallo, and E. Kapon, "Bound-to-continuum terahertz quantum cascade laser with a single-quantum-well phonon extraction/injection stage," New J. Phys. **11**(12), 125022 (2009).
26. C. M. Bledt, J. E. Melzer, and J. A. Harrington, "Fabrication and characterization of improved Ag/PS hollow-glass waveguides for THz transmission," Appl. Opt. **52**(27), 6703–6709 (2013).
27. M. Born and E. Wolf, *Principles of Optics* (Cambridge University, 1999).

1. Introduction

The terahertz (THz) quantum cascade laser (QCL) [1] has great potential in a diverse range of fields, including biomedicine, sensing, security, and quality control [2], in a frequency range that has been traditionally challenging to operate within. THz QCLs offer a high power (up to ~1 W [3]), compact, and frequency selectable radiation source. Currently, maximum operating temperatures have reached 199.5 K in pulsed mode and, by suitable design and growth of the active region, the emission bandwidth can be up to ~1.6 THz [4] from a single device. The understanding of the physics governing the operation of such devices is starting to reach maturity. However, the next generation of challenges involve the effective and efficient implementation of the THz QCL as a radiation source in an ever diversifying range of applications. For successful incorporation, the ability to produce highly collimated, predictable, single lobed emission over meaningful distances (>100 mm), external to the housing cryostat, is a necessity, and to date has proved elusive. Such an achievement would constitute a powerful step away from free space THz optics, and open the way for THz systems to mimic the highly successful move to fibre based systems at 1.55 μm, which has proven so effective in recent decades. This constitutes the primary motivation for this work.

There exists a wide range of THz waveguides currently available with the ability to guide THz beams, each with their own merits and drawbacks. In general, material losses in the THz range are non-negligible, and as such, traditional solid core fibres on the whole perform poorly in terms of intrinsic losses [5]. To overcome this, various alternative fibres have been demonstrated, including photonic bandgap [6], porous [7] and hollow core designs [8]. Here, we choose to work with a hollow flexible polystyrene-lined Ag waveguide (PS-MWG), as characterised in [9], to guide our QCL beam. The dielectric lined hollow core designs stand out as having a number of strengths; broadband transmission with low dispersion (~6 ps/THz·m at 2 THz [10]), relatively low losses (1 dB/m for a 2.2 mm diameter [11]), and the ability to support fundamental low order Gaussian-like modes, such as the HE_{11} mode.

#241983 Received 8 Jun 2015; revised 7 Sep 2015; accepted 8 Sep 2015; published 29 Sep 2015

Flexibility is also possible, even for waveguides fabricated from hollow glass tubes, given that the diameter is not larger than a few mm, after which the structure becomes prohibitively rigid. The challenge for creating an effective delivery system is to efficiently couple the QCL output beam, from the cryostat, to the chosen THz waveguide (WG), external to the cryostat. To achieve this, the choice of WG for the laser itself is a key consideration, as this affects the beam profile to be coupled into the external WG.

For the laser WG, one of two geometries have been typically used - the single plasmon (SP) [1], and metal-metal (MM) [12]. The SP geometry consists of a surface plasmon supporting Au layer above the active region, and a highly doped GaAs layer below, allowing a large mode leakage (~150 μm) into the GaAs substrate. The resulting output powers are generally high (> 100 mW), and mode divergence is low (< 20°). However, the temperature performance is superior in the MM configuration, where the active region is sandwiched between two plasmon supporting Au layers. This however is at the expense of both the power emitted (typically 1-10 mW) and far field pattern, which is generally multi-lobed and highly divergent (> 20°). This is a result of the high degree of subwavelength mode confinement in the laser cavity. Consequently, a method for shaping the emission from a MM QCL is required in order to couple to any external WG efficiently. Previous demonstrations of coupling a QCL into an external fibre have utilised surface emitting micro-ring THz QCLs, coupled into an aluminium cylindrical WG [13] or a silver coated polycarbonate WG [14], both external to the cryostat, with efficiencies of ~98% and ~88% respectively. Coupling to these waveguides was achieved either directly from the facet, or with the aid of an external lens, to excite the TE_{mn} WG modes. Notably, in both works, the optimal spatial profile of the QCL emission was deliberately chosen for high efficiency coupling into the WG. In this work, we demonstrate efficient coupling from a MM QCL, which has an inherently poor quality, highly diffractive beam profile.

In order to match the QCL mode with the external WG, we use a method of controlling the MM QCL beam within the cryostat. Previously demonstrated methods of beam control within the cryostat include 3rd order distributed feedback Bragg (DFB) grating structures [15], which use a periodic grating etched into the top contact of the device, producing a good quality beam profile through constructive interference from successive sections of the device. However, approaches based on this technique are inherently frequency selective, which is restrictive when considering the breadth of potential applications for broadband THz QCLs. Successful broadband attempts at beam shaping include the use of a high resistivity Si lens, attached directly to the laser facet [16], which acts as both an impedance matching medium, as well as a collimating element, antenna-like structures [17–20], or the use of hollow metallic [21] or dielectric [22] waveguides affixed directly to the laser mounting block. These latter attempts represent the foundations on which this work is based.

We demonstrate the excitation of a low divergence HE_{11} Gaussian-like beam at a distance of >500 mm from the facet of a MM THz QCL via the use of a hollow metallic waveguide (MWG) monolithically integrated into the laser mounting block, internal to the cryostat, supporting a TE_{11} mode which is subsequently coupled to a low-loss flexible PS-MWG, external to the cryostat. A high coupling efficiency (>90%) was achieved between the internal MWG and external PS-MWG without the use of any additional optical components, compared to just ~15% between a bare MM QCL and PS-MWG. Additionally, a beam cleaning effect was observed, whereby a sub-optimal, multi-lobed beam exiting the cryostat reverts to the single-lobed HE_{11} mode after transmission through the PS-MWG. A comparison with another commonly used collimating technique, a high resistivity silicon lens attached to the laser facet, was also investigated, and was shown to excite a higher order, non-Gaussian mode from the PS-MWG, and therefore lacked suitability for many applications. Finally, the ability to nitrogen purge the PS-MWG is demonstrated, increasing power transmission by up to 20% over a distance of 555 mm. This paves the way for THz fibre based sensing and spectroscopy applications, which require the introduction and analysis of a gas species in low volumes, similar to techniques already established in the mid-infrared [23].

#241983 Received 8 Jun 2015; revised 7 Sep 2015; accepted 8 Sep 2015; published 29 Sep 2015

2. Integrated hollow copper waveguide

Firstly, we present a technique to shape the beam of MM QCLs, reducing the degree of divergence and creating a Gaussian-like emission, with the aim of producing an effective beam shaping element in its own right, but also as a method of coupling to an external waveguide. Two active region (AR) designs were utilised in this work: a bound-to-continuum (BtC) design emitting at 2.85 THz [24], and a hybrid BtC design which takes advantage of a mini-band of lower lasing states followed by longitudinal optical phonon extraction, first demonstrated by Amanti et al. [25]. The BtC design has many strengths, including the potential to operate in continuous-wave (cw) mode for both SP and MM architectures with a typical bandwidth of ~200 GHz, which is beneficial for applications such as spectroscopy, as well as being well studied and robust to growth errors. Such designs do however suffer from low maximum operating temperatures (~100 K). The hybrid BtC design benefits from a high maximum operating temperature (145 K), and was also chosen to demonstrate the broadband capability of the WG system, emitting with a large bandwidth of ~400 GHz around 3.2 THz.

The beam shaping technique expanded in this work is based on the use of a hollow MWG, originally demonstrated in [21], whereby a cylindrical hollow copper WG, 1.7 mm in diameter, was affixed directly to the laser mounting block with the aid of a UV sensitive adhesive. When aligned with a MM QCL, the TE_{11} mode of the waveguide was excited, producing a Gaussian-like beam with a half divergence angle of ~3.7°. The approach, while effective at demonstrating an improvement in beam quality and collimation, was unsuitable for achieving efficient coupling to a further external flexible WG due to the large 1.7 mm diameter, and also suffered from mechanical fragility. In this work, we address these considerations by monolithically integrating a hollow MWG directly into the laser mounting block, allowing the internal diameter to be chosen for mode matching to a further WG.

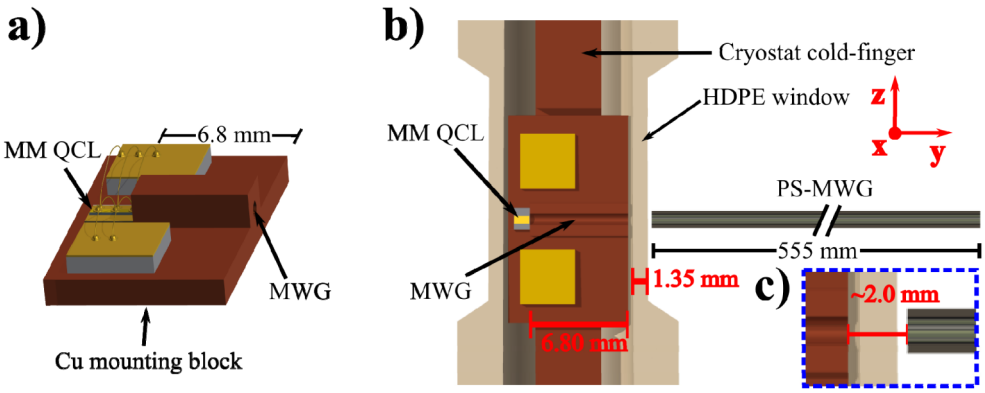

Fig. 1. a) Schematic of the integrated MWG, showing the MM QCL indium bonded parallel with the central axis of a 6.8 mm long hollow cylindrical waveguide monolithically incorporated into the mounting block. b) Schematic cross-sectional view of the setup to couple the integrated MWG to the external PS-MWG. The lengths of the MWG and PS-MWG are 6.80 and 555 mm respectively, and the thickness of the HDPE window is 1.35 mm. c) Inset showing the ~2.0 mm separation between the MWG and PS-MWG.

MM QCLs were processed using standard thermo-compression bonding and wet etching techniques to produce ridge lasers of 12 µm height, 130 µm width and 0.5 - 1.5 mm length. The integrated MWG was fabricated by taking a rectangular copper mounting block of dimensions 19 × 9.75 × 1.5 mm and fabricating a 1 mm diameter, 6.8 mm long cylindrical WG, positioned such that the central axis was 0.5 mm above the mounting plane of the laser [see Fig. 1(a)]. This height was chosen such that the facet of the QCL was automatically aligned with the central waveguide axis in the vertical direction (± 25 µm), accounting for the GaAs substrate. Alignment was performed under a microscope to ensure the central axis of the ridge and waveguide were parallel and aligned (estimated error on alignment of ± 50 µm). The length of the waveguide was chosen to allow the formation of the TE_{11} mode of the

#241983 Received 8 Jun 2015; revised 7 Sep 2015; accepted 8 Sep 2015; published 29 Sep 2015

structure, whilst also delivering a Gaussian-like beam to the inside edge of the cryostat window. Devices were mounted onto the cold finger of a continuous flow He cryostat, with a cylindrical high density polyethylene (HDPE) window of inner diameter 12 mm and 1.35 mm wall thickness. Once mounted, the distance between the end of the MWG and inside of the window was ~0.5 mm. Devices were operated in pulsed mode at 100 kHz and 2% duty cycle, as well as being gated at 7 Hz to allow lock-in detection of power with a Golay cell detector. A number of devices were fabricated, with typical back-facet absolute powers of 2 – 3 mW for the hybrid BtC AR (corrected for 100% duty cycle operation).

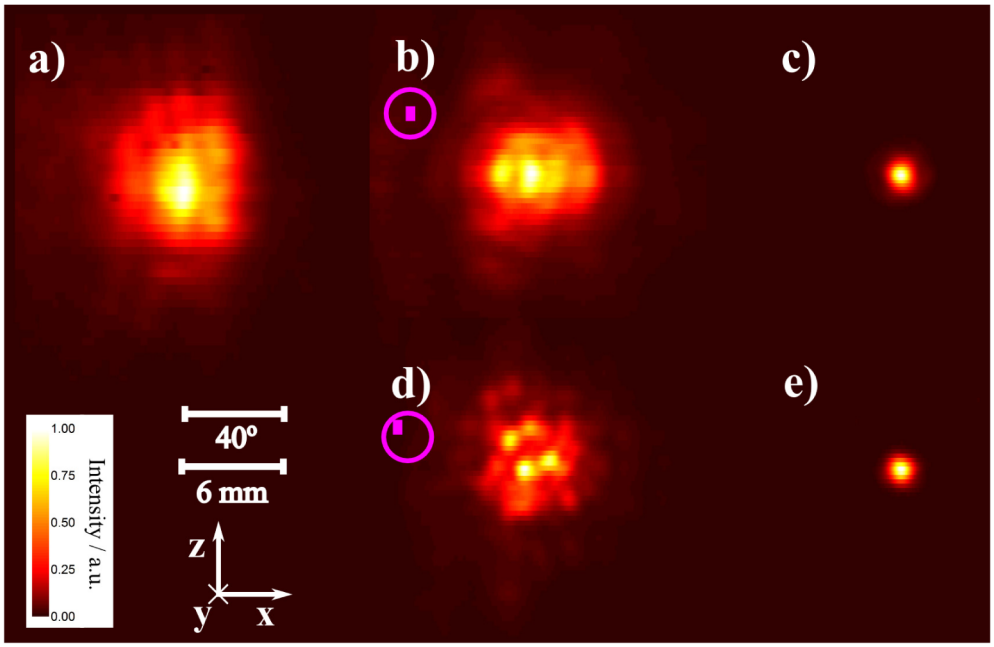

Fig. 2. Beam profiles of the integrated MWG device with hybrid BtC AR, acquired using a Golay cell with a 1 mm aperture, scanned in the plane perpendicular to the beam. Profiles are normalised to their individual peak powers. a) Beam profile acquired at a distance of 7 mm from the rear facet of the device b) Beam profile acquired at a distance of 7 mm from the end of the MWG c) Beam profile measured at 7 mm from the end of the PS-MWG, exhibiting the HE_{11} mode d) Beam profile of the integrated WG device with the laser deliberately misaligned by ~150 μm in both x and z directions, acquired at 7 mm from the end of the WG e) Beam profile measured at 7 mm from the end of the PS-MWG after excitation by misaligned device, still exhibiting the HE_{11} mode.

In order to investigate the potential influence on the maximum operating temperature of the device as a result of the introduction of additional copper on the heat-sink, the maximum temperature at which lasing occurred was recorded for devices of identical active region mounted both on a standard copper block, and the integrated Cu waveguide block. Maximum operating temperatures were found to be 75 K versus 80 K for the integrated waveguide and standard device respectively in the case of the BtC AR, and 133K versus 145K for the hybrid BtC AR, suggesting the increase in heat load minimally affects the temperature operation in each case. Next, the effect of the MWG on the beam profile of the device was investigated by utilising a Golay cell detector with a 1 mm aperture added to improve spatial resolution. The detector was mounted on a motorised x-y stage, and raster scanned in the plane perpendicular to the beam (x-z plane) at a distance of 7 mm from both the back facet of the device, and the end of the front of the MWG. A distance of 7 mm was chosen to maintain sufficient power for detection with a 1 mm aperture, whilst also allowing sufficient divergence to fully reveal the spatial characteristics of the mode. Representative results for a hybrid BtC AR device are displayed in Figs. 2(a) and 2(b) respectively, acquired with a 0.3 mm step size. The profile

#241983 Received 8 Jun 2015; revised 7 Sep 2015; accepted 8 Sep 2015; published 29 Sep 2015

from the back facet displays a high degree of divergence (half angle > 30°) in both spatial directions [see Fig. 2(a)]. The profile divergence is better than typically observed for MM QCLs most likely as a result of back-plane reflection from the mounting block [20]. Upon passing through the MWG, a clear improvement is demonstrated [Fig. 2(b)], with the degree of divergence reduced (half angle ~23° in the x and ~20° in the z direction), and evidence of the formation of the TE_{11} mode of the structure observed from the Gaussian-like power profile. A higher degree of divergence in the x direction is most likely due to the asymmetry of the laser facet. The coupling efficiency into the MWG was also estimated. Emitted powers from both the back facet and MWG of a hybrid BtC AR device were collected using a pair of off-axis parabolic mirrors (f = 50 and 101 mm respectively), and a large area (5 mm^2) pyroelectric detector, yielding a maximum efficiency of 70 ± 5%, assuming negligible losses through the 6.8 mm waveguide.

The integrated MWG approach possesses many strengths when attempting to couple a MM QCL to a further external WG. The increased mechanical stability of the structure is particularly beneficial when loading devices into the cryostat over successive thermal cycles. This increased stability also facilitates ease of alignment between laser and WG, allowing incremental improvements by heating the device, melting the indium bond, and realigning. Additionally, the diameter of the MWG can easily be varied by suitable design, allowing the spatial beam distribution to be readily matched to that of a further WG, placed externally to the cryostat window. In this work, the 1 mm diameter MWG was chosen to efficiently couple to a 1 mm internal diameter flexible PS/Ag WG, which forms the subject of the following section.

3. Coupling to flexible Ag/PS hollow waveguide

In this section, we demonstrate the ability to couple the integrated MWG, outlined above, into an external dielectric-lined hollow metallic waveguide. The external waveguide is constructed from a 1 mm diameter fused silica capillary with a ~0.6 μm thick layer of silver deposited on the inner walls. Onto this, a 10 μm thick layer of polystyrene (PS) is additionally deposited [26]. The thickness of the dielectric layer determines the primary transmission band of the structure, designed here for frequencies around 3 THz. Finite element analysis simulations show a significant spatial overlap between the TE_{11} mode of the MWG and the HE_{11} mode of the PS-MWG at a separation of 3 mm [see Fig. 3], for the case of a 1 mm diameter for each WG. The 1 mm diameter for the MWG was chosen as it allows the best coupling to the PS-MWG, which has a fixed 1 mm diameter. A smaller MWG diameter would yield a tighter spot, but also an increased divergence. Given that our experimental setup was limited to 2 – 3 mm in relative distance, the 1 mm diameter proved the best compromise between these conflicting considerations, and provided an optimal mode overlap. This high overlap is due to the Gaussian-like nature of both the TE_{11} and HE_{11} modes, despite minor deviations in the case of the TE_{11} mode, mostly in the x direction [see Fig. 3(b)]. These simulations suggest that a coupling efficiency > 80% can be achieved if the waveguides are brought to within a distance of 3 mm, and efficiencies > 90% are possible for a separation of 2 mm or less. The experimental procedure conducted to achieve this is outlined below.

A PS-MWG of length 555 mm was mounted on micrometre stages and brought to within 0.3 mm of the outside of the 1.35 mm thick HDPE window, and aligned with the axis of the MWG situated ~0.5 mm inside the cryostat window, making a total distance between internal and external waveguides of ~2 mm, and total distance from laser facet to end of PS-MWG of ~564 mm [see Fig. 1(b)]. The beam profile exiting the PS-MWG was measured in the same manner as outlined for the MWG, with the aperture of the Golay cell detector at a distance of 7 mm from the end of the PS-MWG. The resulting profile from the same device used in Figs. 2(a) and 2(b) is shown in Fig. 2(c), acquired with a 0.15 mm step size. Excitation of the Gaussian-like HE_{11} mode of the structure can clearly be observed, with a beam waist of 1.00 mm. Also shown in Fig. 2 is the effect of misalignment of the laser with respect to the MWG

#241983 Received 8 Jun 2015; revised 7 Sep 2015; accepted 8 Sep 2015; published 29 Sep 2015

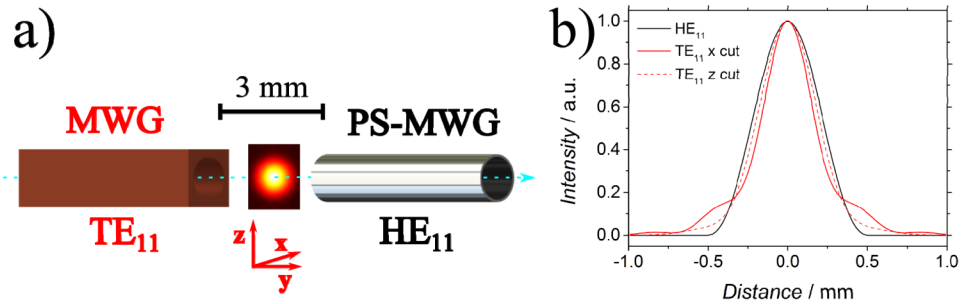

Fig. 3. a) Schematic of the calculation of the mode overlap between the TE_{11} mode of the MWG, internal to the cryostat, and the HE_{11} mode of the external PS-MWG at a separation of 3 mm. b) Comparison of line cuts from the simulated TE_{11} mode in x and z directions at a distance of 3 mm from the exit of the MWG, and the symmetric HE_{11} mode at the entrance to the PS-MWG, showing a high degree of overlap (> 80%).

on the resultant beam profiles from both internal and external waveguides. Figure 2(d) shows the beam profile acquired at a distance of 7 mm from the end of the MWG, with the laser deliberately mounted approximately 150 µm away from the central axis in both the x and z directions. A quadrupole output is observed, suggesting that a higher order mode of the structure is excited due to the sub-optimal alignment, which can arise due to the relatively low propagation losses of higher order modes in such short metallic waveguides [21]. The quadrupole mode was subsequently coupled into the PS-MWG, resulting in the excitation of the HE_{11} mode only [Fig. 2(e)]. Thus we observe a beam cleaning effect using the MWG approach, whereby a sub-optimal input mode, upon transmission through the PS-MWG, is still capable of exciting the desirable Gaussian-like HE_{11} mode.

To estimate the coupling efficiency between the MWG and PS-MWG, the emitted power with and without the PS-MWG was collected from a hybrid BtC AR device using a pair of off-axis parabolic mirrors (f = 50 and 101 mm) and a large area (5 mm^2) pyroelectric detector, which, accounting for the ~5dB/m losses of the waveguide, yielded an efficiency of 80 ± 5%, uncorrected for atmospheric absorption. Additionally, in order to verify the necessity of the internal MWG, a comparison was made by coupling a bare MM QCL directly into the PS-MWG. A laser was mounted on a standard copper block and positioned such that the facet was ~0.5 mm from the inside of the cryostat window. Although the HE_{11} mode was still excited, the coupling efficiency was estimated to be ~15 ± 5%, demonstrating that a 4 fold increase in power transmission was obtained when using the MWG approach, accounting for coupling losses into both internal and external waveguides.

In order to investigate further the HE_{11} beam profile emitted from the PS-MWG, line-cuts in both x and z directions were taken for a profile acquired at 4.5 mm from the PS-MWG [see Figs. 4(a)-4(c)]. From standard Gaussian optics theory, the transverse beam profile is given by [27]:

$$P(x,y) = P_0\left(\frac{w_0}{w(y)}\right)^2 e^{\left(\frac{-2x^2}{w^2(y)}\right)} \quad (1)$$

where P_0 is the power at the centre of the beam at w_0, the minimum beam waist, w(y) is the beam waist at distance y away from the minimum and x (or z for a spatially symmetric beam) is the transverse distance from the beam centre. Fitting the x and z line-cuts with Eq. (1) demonstrates that the HE_{11} beam is well approximated by a Gaussian beam, which is expected due to the beam diameter being substantially larger than the free space wavelength (λ≈100 µm), and the wavefront being approximately flat. To determine the divergence of the beam, profiles were taken at 4.5, 7.0, 10.0 and 20.0 mm from the end of the PS-MWG, which were then fitted with Eq. (1) [Fig. 4(d)]. Taking the beam waists as the distance between the maximum power and the point where the power drops to $1/e^2$ of the maximum value, the

#241983 Received 8 Jun 2015; revised 7 Sep 2015; accepted 8 Sep 2015; published 29 Sep 2015

experimental divergence half angle was calculated to be ~7°. From Gaussian optics, the theoretical divergence half angle, θ, is approximately given by

$$\theta \simeq \frac{\lambda}{\pi w_0} \tag{2}$$

where λ is the wavelength, and w_0 is the beam waist of the HE_{11} mode exiting the PS-MWG (0.38 mm), producing a theoretical beam divergence half angle of ~5°. The agreement between the theoretical and experimental values is good, and the discrepancy can be attributed to the use of a 1 mm aperture to record the beam profiles, which may have the effect of extending the experimental profiles laterally, as well as the error in recording the separation between PS-MWG and detector (~0.5 mm). The beam quality factor, M^2, was also estimated to be 1.21. The demonstrated divergence of ~7° from a 1 mm diameter waveguide is consistent with previously reported values, including 3.7° for a 1.8 mm diameter copper waveguide, and 10° for a 3 mm diameter silicon lens [21]. Spectral analysis was also conducted using a Fourier transform infrared spectrometer with bolometric detection, which showed that the mode content of the initial laser spectrum was preserved upon transmission through both the MWG and the PS-MWG, in both the active regions tested (not shown).

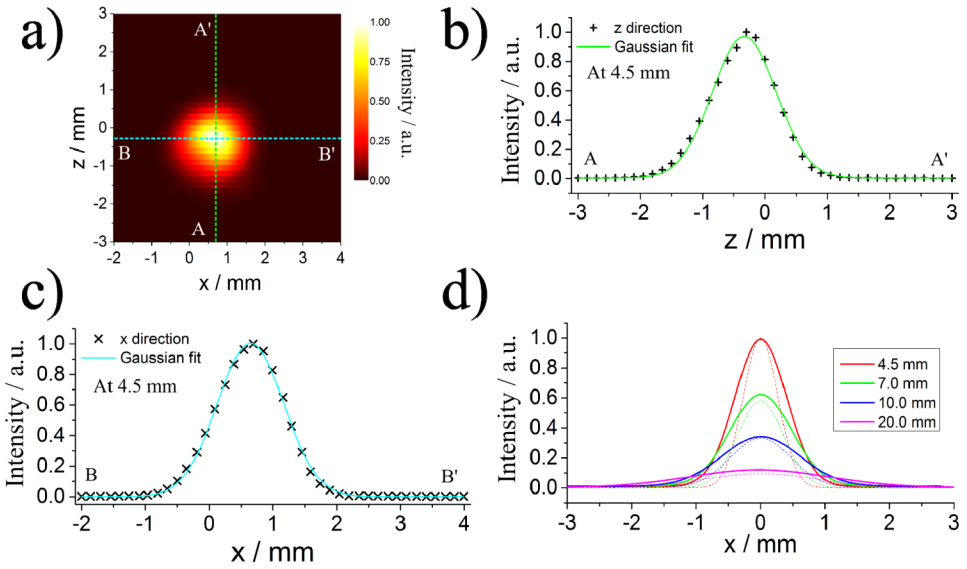

Fig. 4. a) Normalised beam profile measured at 4.5 mm from the PS-MWG, showing excitation of the HE_{11} mode. b) Gaussian fit of the experimental beam profile in the vertical (z) direction. c) Gaussian fit of the experimental beam profile in the horizontal (x) direction. d) Gaussian fits of experimental beam profiles, taken in the x direction at 4.5, 7.0, 10.0 and 20.0 mm from the PS-MWG, showing a divergence half angle of ~7°. The dashed lines show the theoretical divergence calculated using Gaussian optics (~5°).

4. Comparison between MWG and silicon lens

Thus far, we have demonstrated how the use of an integrated MWG allows efficient coupling of MM QCLs into an external PS-MWG. One of the alternatives which is commonly employed for beam shaping within the cryostat is the high resistivity silicon lens, which is attached directly to the laser facet, and has been shown to act well as both an impedance matching and collimating technique, increasing power output by a factor of 4 or more [16]. The effectiveness of such a technique for coupling into the external waveguide is explored in this section, to allow a comparison to be drawn with the MWG method outlined above.

#241983 Received 8 Jun 2015; revised 7 Sep 2015; accepted 8 Sep 2015; published 29 Sep 2015

A 3 mm diameter hyper-hemispherical high resistivity silicon lens with 0.6 mm spacer was attached to the facet of a MM QCL under a microscope using a UV sensitive adhesive. The device was mounted such that the end of the lens was 0.5 mm from the inside of the HDPE window, to allow coupling of the emitted power into the external PS-MWG in the same manner as described previously. With the addition of the lens, the output power of the laser was increased by a factor of 4. To determine the coupling efficiency, the emitted power with and without the PS-MWG was collected with a pair of off-axis parabolic mirrors (f = 50 and 101 mm) and a large area pyroelectric detector. Accounting for the waveguide losses, a coupling efficiency of 70 ± 5% was calculated, unadjusted for atmospheric absorption. The beam profile exiting the PS-MWG was measured with a Golay cell detector with 1 mm aperture at a distance of 7 mm from the waveguide end, and is shown in Fig. 5 alongside the mode measured at the same distance when using the MWG as the exciting element. A higher order mode is clearly observed from the PS-MWG when excited by the silicon lens QCL, exhibiting a bi-lobed annular distribution, with a higher degree of divergence compared to the HE_{11} mode. We postulate this higher order mode excitation to be a result of the optical mismatch between the input mode and the HE_{11} PS-MWG mode to be excited. The elliptical nature of beam profiles produced by silicon lens QCLs, resulting from the asymmetric nature of the laser resonator cross-section, produce a sub-optimal spatial distribution of power coupled into the PS-MWG. Such higher-order mode excitation is clearly detrimental from an application standpoint, as single lobed emission is almost unilaterally required.

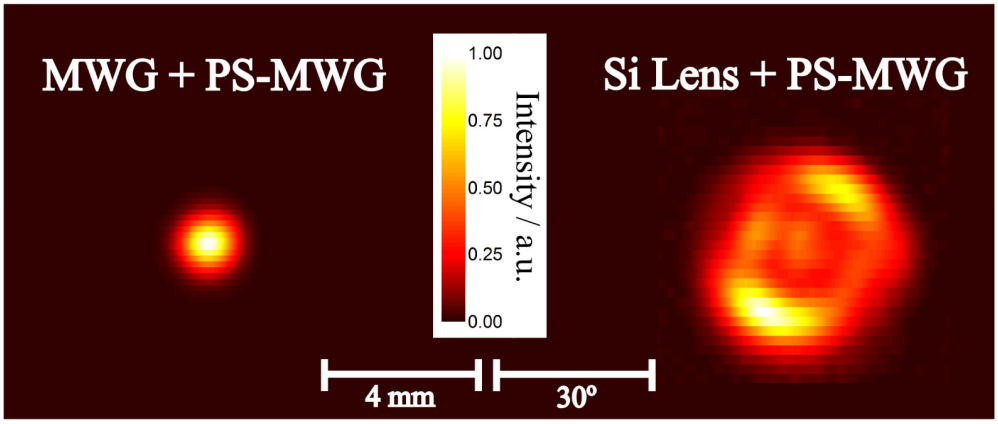

Fig. 5. Comparison of beam profiles acquired at 7 mm from end of PS-MWG, upon excitation from the MWG (left) and silicon lens QCL (right), with an angular, bi-lobed higher order mode excited in the latter case. Each profile is normalised to its own peak value.

Any application will require the ability to confidently excite the fundamental HE_{11} mode at every optical setup, without the need to confirm through additional measurements. With this in mind, the reliability of the excitation of the HE_{11} mode using the MWG approach was investigated. Figure 6(a) shows the effect on the PS-MWG mode excitation resulting from deliberate misalignment between the MWG and PS-MWG in the lateral x direction. Beam profiles were acquired at 4.5 mm from the PS-MWG end, with the two waveguides displaced by 0, 0.5, and 1.0 mm respectively. As can be seen, despite some minor aberrations in the spatial symmetry, the Gaussian-like HE_{11} mode is clearly excited in all cases. We attribute this to the well matched spatial power distributions of the TE_{11} and HE_{11} modes of the two waveguides, which promotes preferential excitation primarily of the fundamental HE_{11} mode. As discussed above, with a mind towards future applications, this reliable ability to excite the fundamental mode is clearly advantageous, especially in systems requiring regular disassembly and re-alignment.

Another important future application consideration is the tolerance of power transmission to partial misalignment of the exciting element into the PS-MWG. Here we investigate this by

#241983 Received 8 Jun 2015; revised 7 Sep 2015; accepted 8 Sep 2015; published 29 Sep 2015

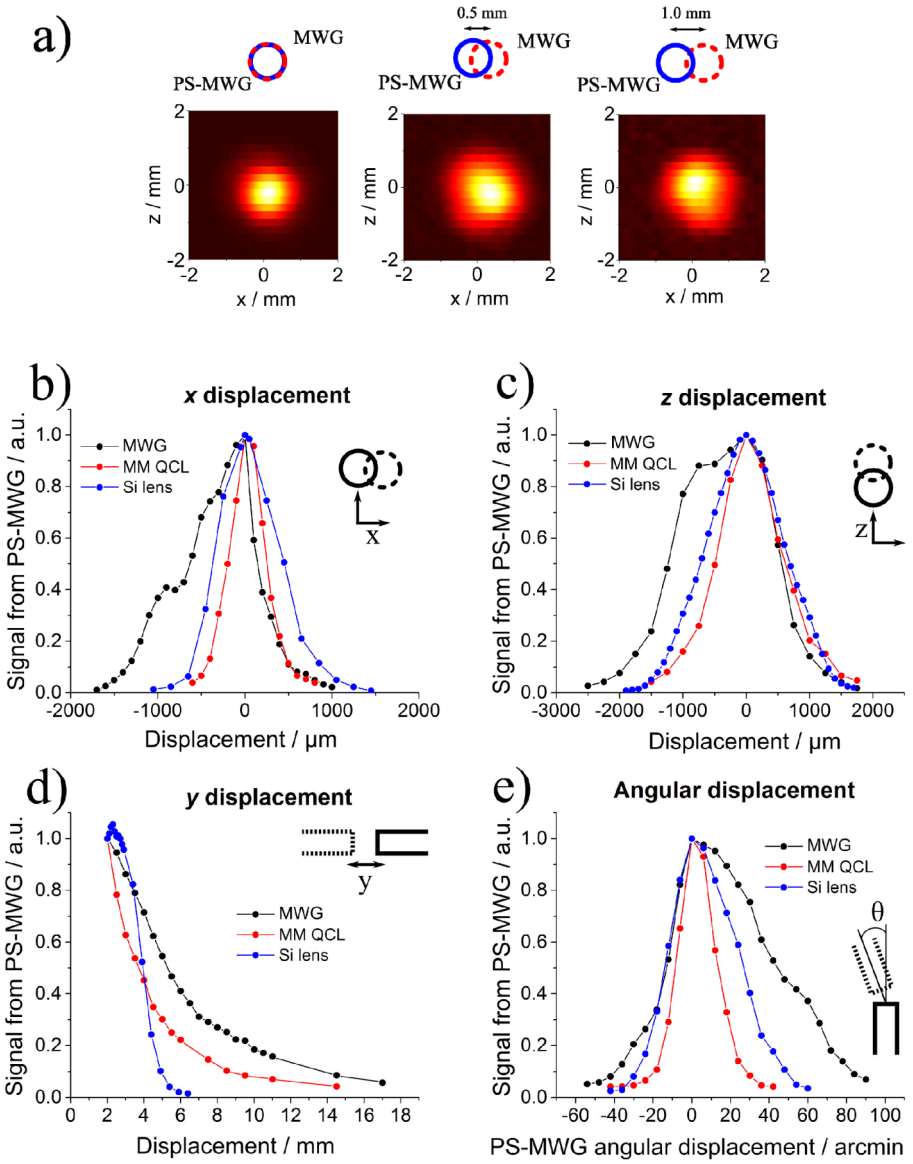

Fig. 6. a) Effect of MWG misalignment on PS-MWG mode excitation, with misalignment of 0, 0.5 and 1.0 mm in the x direction respectively. Beam profiles were acquired at 4.5 mm from the PS-MWG end, and each normalised to their peak power values. The excitation of the HE_{11} mode is maintained in each case, and is also the case for displacement in the z direction. b) Normalised power transmission through PS-MWG for the three cases of excitation – bare MM QCL, MWG and Si lens, as a function of displacement of the exciting element in the x direction. c) Normalised power transmission as a function of displacement in the z direction. d) Normalised power transmission as a function of separation from PS-MWG (y displacement) e) Normalised power transmission as a function of PS-MWG rotation in x-y plane. In all cases, a similar or greater tolerance for misalignment is observed for the MWG.

recording the power transmission from the PS-MWG whilst incrementally misaligning the exciting element, in each spatial direction, as well as rotationally in the x-y plane [see Fig. 1 for axes definition]. Normalised graphs of power versus displacement are shown in Fig. 6 for each direction, for all excitation scenarios discussed above - a bare MM QCL, the MWG and the silicon lens QCL. For the x direction, the MWG and silicon lens show a similar distance to

#241983 Received 8 Jun 2015; revised 7 Sep 2015; accepted 8 Sep 2015; published 29 Sep 2015

half power of 400 µm, approximately twice that for the bare laser. In the z direction, the MWG shows 200 µm larger tolerance in power transfer compared to the other two techniques, and in angular displacement shows a clear advantage, with a distance to half power of 0.5° compared to 0.3° in the silicon lens case. Finally, for increasing separation from the PS-MWG, the slowest drop-off in power is clearly observed for the MWG (5.3 mm to half power), with the silicon lens demonstrating a different trend, indicative of the excitation of a higher order mode already discussed. The power transmission increases by ~8% within 0.5 mm, then falls off rapidly to zero within 7 mm of separation from the PS-MWG. This can be ascribed to the higher degree of power delivered at the PS-MWG edges in the case of the higher order mode, providing a smaller area for excitation, and thus a more rapid power transmission drop with increasing separation. In all cases, a similar or greater tolerance for misalignment is observed for the MWG, due to the high degree of mode matching between waveguides, as well as the superior divergence compared to a bare laser. This represents a clear advantage when assembling future THz systems, especially when minimising the separation from the external waveguide, which is particularly challenging at cryogenic temperatures, where cryostat configurations become a primary concern, and given the lack of low-loss THz materials currently available.

5. Nitrogen purging of external waveguide

For most applications, the power transmission dramatically influences the signal to noise of the system. One major factor which typically hampers transmission, particularly over distances >100 mm, is the broadband THz absorption of atmospheric water vapour. In fact, the degree to which a source frequency overlaps with a transmission window plays a far greater role in system viability than the original source power. Consequently, a method for simply and effectively purging the atmospheric water content from the PS-MWG using gaseous nitrogen is demonstrated here. The setup is shown schematically in Fig. 7(a). An aluminium holder was designed to support the exit end of the PS-MWG, with the purpose of simultaneously allowing THz transmission, whilst also introducing a pure N_2 atmosphere into the hollow interior of the waveguide. This was achieved using a 12.5 µm thick film of low density polyethylene across the waveguide exit, allowing transmission with negligible loss, whilst being simultaneously airtight.

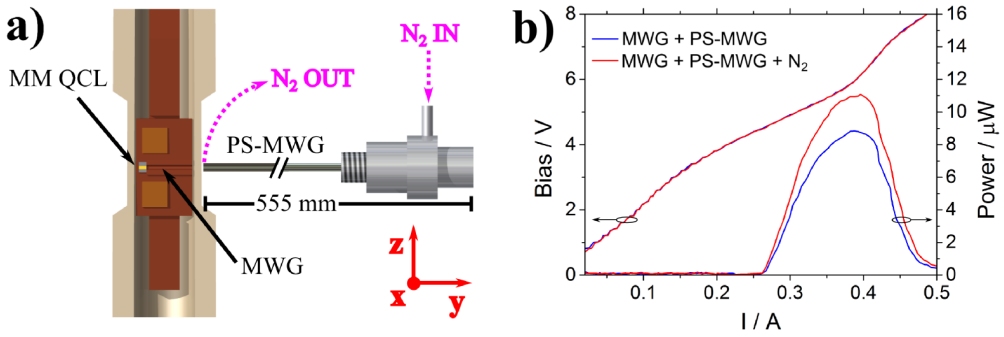

Fig. 7. a) Schematic of the setup used to purge the PS-MWG, showing the direction of N_2 flow. The QCL was held at 4.5 K and pulsed at 100 kHz and 30% duty cycle b) Exemplar light-current-voltage graph of transmitted power through the PS-MWG, under excitation from the MWG, without N_2 purge (blue) and with N_2 purge (red), with bias voltage on the left-hand axis and transmitted power on the right-hand axis. An increase in power of ~20% is observed.

An exemplar plot of emitted power and bias voltage versus current is displayed in Fig. 7(b), for the PS-MWG in two cases - under excitation from a 130 × 500 µm BtC AR copper waveguide device in the absence of N_2 purging, and in the presence of N_2 purging. A single mode 2.85 THz BtC device was chosen, as narrow width emission centred even partly on an atmospheric absorption line is a traditional hindrance to long range power transmission in many system designs. Power was collected using a pair of off-axis parabolic mirrors (f = 50

#241983 Received 8 Jun 2015; revised 7 Sep 2015; accepted 8 Sep 2015; published 29 Sep 2015

and 101 mm) and a large area pyroelectric detector. An increase in peak power of ~20% was observed, which was calculated from an average of 3 separate purging runs, each from an initial relative humidity of 38%. The coupling efficiency for the MWG into PS-MWG was also measured in the absence of water vapour, yielding a final value of > 90%, accounting for the PS-MWG losses.

This demonstration of the ability to introduce amounts of a gaseous species into the core of the PS-MWG is hypothetically more beneficial as one transfers to ever-increasing optical path lengths, and the 555 mm waveguide used in this work was chosen for merely demonstrative purposes. Due to the comparatively low WG loss at typical QCL frequencies, the system shown here could be increased in length to many metres or more without the requirement for delicate optical alignments, yielding substantial benefits in transmission and sensitivity from the ability to selectively purge the system with a minimal quantity of gas. Existing techniques which could benefit from this work include external cavity tuning and frequency locking of QCLs, whereby the easily purged environment has the potential to decrease attenuation and instances of mode-hopping induced by specific absorption lines. This work also paves the way for a new generation of THz systems, already established at mid-IR frequencies, where fibre-based spectroscopic systems exhibit high response times and require notably small test volumes as a result of the PS-MWG being almost instantaneously filled, as well as the high spatial overlap between the optical mode and the test gas species, the interaction length of which can be readily extended with ease [23].

6. Conclusion

In this work we have demonstrated flexible and predictable power delivery from a MM THz QCL over a distance >500 mm, through the use of an integrated copper waveguide, internal to the cryostat, and a flexible dielectric lined hollow waveguide external to the cryostat. We estimate a coupling efficiency between the internal and external waveguides >90%, which is approaching the theoretical maximum. A single-lobed Gaussian-like HE_{11} mode emission is observed at a distance of 564 mm from the laser facet, which is robust to alignment errors when compared to other excitation methods, such as a bare laser or silicon lens QCL. Also demonstrated is an effective method of purging the external waveguide, increasing power output by up to 20%. This ability to introduce gaseous species into such a long and confined optical path sets the stage for a range of future sensing and spectroscopic applications which are as yet unexplored in the THz frequency range.

Acknowledgments

The authors acknowledge financial support from the Engineering and Physical Sciences Research Council (Grant No. EP/J017671/1, Coherent Terahertz Systems). Additional data sets related to this publication are available from the Cambridge University data repository at https://www.repository.cam.ac.uk/handle/1810/249004.